

Article

Valorization of Rice Husk for the Production of Porous Biochar Materials

Wen-Tien Tsai ^{1,*}, Yu-Quan Lin ¹ and Hung-Ju Huang ²

¹ Graduate Institute of Bioresources, National Pingtung University of Science and Technology, Pingtung 912, Taiwan; wsx55222525@gmail.com

² General Research Service Center, National Pingtung University of Science and Technology, Pingtung 912, Taiwan; redbull@mail.npust.edu.tw

* Correspondence: wtsai@mail.npust.edu.tw; Tel.: +886-8-770-3202

Abstract: Rice husk (RH) is one of the most important crop residues around the world, making its valorization an urgent and important topic in recent years. This work focused on the production of RH-based biochars at different pyrolysis temperatures from 400 to 900 °C and holding times from 0 to 90 min. Furthermore, the variations in the yields and pore properties of the resulting biochars were related to these process conditions. The results showed that the pore properties (i.e., BET surface area and porosity) of the resulting RH-based biochar were positively correlated with the ranges of pyrolysis temperature and holding time studied. The maximal pore properties with a BET surface area of around 280 m²/g and porosity of 0.316 can be obtained from the conditions at 900 °C for a holding time of 90 min. According to the data on the nitrogen (N₂) adsorption–desorption isotherms and pore size distributions, both microporous and mesoporous structures exist in the resulting biochar. In addition, the EDS and FTIR analyses also supported the slight hydrophilicity on the surface of the RH-based biochar due to the oxygen/silica-containing functional groups. Based on the findings of this work, the RH-based biochar could be used as a material in environmental applications for water conservation, wastewater treatment and soil amendment.

Keywords: rice husk; pyrolysis; porous biochar; pore property; surface composition



Citation: Tsai, W.-T.; Lin, Y.-Q.; Huang, H.-J. Valorization of Rice Husk for the Production of Porous Biochar Materials. *Fermentation* **2021**, *7*, 70. <https://doi.org/10.3390/fermentation7020070>

Academic Editor: Alessia Tropea

Received: 31 March 2021

Accepted: 27 April 2021

Published: 30 April 2021

Publisher's Note: MDPI stays neutral with regard to jurisdictional claims in published maps and institutional affiliations.



Copyright: © 2021 by the authors. Licensee MDPI, Basel, Switzerland. This article is an open access article distributed under the terms and conditions of the Creative Commons Attribution (CC BY) license (<https://creativecommons.org/licenses/by/4.0/>).

1. Introduction

The most common biomass feedstocks for the production of energy and carbon materials are plant, wood, agricultural waste or crop residues, which are mainly composed of water, lignocellulosic components (lignin, hemicellulose and cellulose), extractives and ash [1]. Notably, the energy-containing biomass is derived from the sun by converting atmospheric carbon dioxide (CO₂) and water into carbohydrates (or lignocelluloses) through photosynthesis, thus mitigating greenhouse gas (GHG) emissions by displacing fossil fuel use. In this regard, the valorization of biomass for fuels and chemicals was motivated mainly by the benefits of renewable resources, global warming (environmental protection) and social economy [1]. For example, biomass has been considered as a carbon-neutral feedstock or fuel from the viewpoint of the carbon cycle principle regarding the environment. Furthermore, biomass can be converted by biochemical and thermochemical methods into useful products [2]. Pyrolysis, one of the commonly used thermochemical conversion processes, involves decomposition of biomass in the absence of air or oxygen at an elevated temperature [3]. The resulting biochar can be further used as solid fuel, carbon material, soil amendment, environmental adsorbent (biosorbent), functional catalyst or feedstock for chemicals, depending on its final applications [4–9].

In Asia, rice is the most important crop, suggesting that rice husk is an important crop residue because it accounts for around 20% of grain weight. Approximately 150 million metric tons of rice husk are produced annually based on the world production of paddy rice (i.e., 750 million metric tons) [10]. According to the agricultural statistics [11], it was thus

estimated that around 0.4 million metric tons of rice husk are generated annually in Taiwan. Due to its richness in silica and lignocellulosic constituents [12], the biomass is currently used for bioenergy (or solid fuel) in rice milling plants, as a paving/bedding material in poultry farms, animal feed and as a soil amendment in different forms in agricultural lands to increase soil fertility and crop productivity [13–15]. Rice husk is directly reused without converting it into useful materials by thermochemical or biochemical processes. As compared to uncontrolled burning on fields, these direct reuse approaches do not valorize the energy content of the material and may generate toxic emissions without leading to valuable applications such as porous carbon materials.

In order to increase the pore properties, mediate environmental pollution and also mitigate the carbon dioxide release as GHG forms by valorizing rice husk, the potential to enhance the porous structure of resulting biochar products at limited pyrolysis conditions has been widely investigated [16–26]. Vassileva et al. pyrolyzed rice husk at 250, 350, 480 and 700 °C at a heating rate of 4 °C/min and subsequently maintained this temperature for 4 h [16]. Jindo et al. charred rice husk for 10 h at different temperatures (400–800 °C) at a heating rate of 10 °C/min [17]. Phuong et al. investigated the effects of pyrolysis temperature (350, 450 and 550 °C) and heating rate (10 and 50 °C/min) on the yield and properties of the resulting biochar derived from rice husk [18]. Ahiduzzaman and Sadrul Islam produced rice husk biochar at 650 °C for 60 min, which was further activated to produce activated carbon [19]. Wei et al. prepared rice husk biochars at 300, 500 and 750 °C, which were used as adsorbents for comparing the adsorption performance of herbicide metolachlor with their physicochemical characteristics [20]. Zhang et al. reported the physicochemical properties of rice husk biochars prepared under different temperatures (200–800 °C) at a fixed heating rate of 10 °C/min and then kept for 60 min [21]. Dissanayake et al. conducted pyrolysis experiments on rice husk at 350, 500 and 650 °C at a heating rate of 10 °C/min [22]. In this case, the experiment at 350 °C took around 2 h to complete pyrolysis, while the experiments at 500 °C and 650 °C completed the process in around 25 min after reaching the pyrolysis temperature. Jia et al. produced rice husk biochar under 300, 400, 500, 600 and 700 °C (heating rate of 15 °C/min) for 3 h [23]. Shi et al. investigated adsorption interactions between lead ion and biochars produced at 300, 500 and 700 °C [24]. Singh et al. used rice husk biochars, prepared at 300, 450 and 600 °C, as adsorbents of nutrient nitrogen (i.e., urea), showing the huge sorption potential of the biochar due to high functionality and porosity [25]. Saeed et al. performed a pyrolysis experiment at a constant temperature of 500 °C for 60 min [26]. It is clear that the pore properties of rice husk biochar will be more developed at higher pyrolysis temperatures because of the greater formation of turbostratic crystallites [27]. Regarding the applications of rice husk biochar, it has been used as an effective adsorbent for the removal of trichloroethylene [28], a good medium for the growth of soursop (*Annona muricata* L.) seedlings [29] and a soil amendment for increasing nutrient retention [30,31].

In Taiwan, rice husk biochar has been extensively applied to agricultural soils for enhancing soil fertility and crop yields in recent years due to the promotion of organic farming [30]. However, these biochars showed poor pore properties [32]. For example, the values of the Brunauer–Emmett–Teller (BET) surface area were lower than 5 m²/g. In addition, few studies on the production of rice husk biochar at higher temperatures (e.g., 900 °C) for different holding times have been reported in the literature, as mentioned above. Therefore, this work focused on investigating the variations in the yields and pore properties of rice husk biochar in the pyrolysis process as a function of temperature (400, 500, 600, 700, 800 and 900 °C) and residence time (0, 30, 60 and 90 min) at a commonly used heating rate (10 °C/min). The instrumental analyses, including nitrogen adsorption–desorption isotherms, true density (gas pycnometry using helium displacement principle), scanning electron microscopy–energy-dispersive X-ray spectroscopy (SEM–EDS) and Fourier-transform infrared spectroscopy (FTIR), were performed to determine the physicochemical properties of the resulting rice husk biochar.

2. Materials and Methods

2.1. Material

Rice husk (RH), used as a precursor for producing biochar, was obtained from an agricultural research and extension station (Pingtung County, Taiwan). The as-received biomass was cut by a rotary knife-type shredder. The shredded RH was further sieved to a broad range of mesh screen sizes, ranging from mesh no. 20 (opening size of 0.841 mm) to mesh no. 40 (opening size of 0.420 mm). The sieved RH was first dried in a forced air-circulation oven and then used for the pre-pyrolysis test involving thermogravimetric analysis (TGA) and the pyrolysis experiments. In line with the previous study [33], the dried RH contained high contents of carbon (45.28 wt%), hydrogen (5.51 wt%), oxygen (~44 wt%, estimated) and silicon (3.90 wt%), indicating that this biomass has a moderate calorific value (16.4 MJ/kg) [12].

2.2. Pre-Pyrolysis Test via Thermogravimetric Analysis (TGA)

In order to obtain the proper pyrolysis temperature range of the dried RH, a thermal analyzer (TGA-51; Shimadzu Co., Japan) was used to obtain the TGA data. Around 0.2 g of the RH sample was placed on a quartz crucible and then heated externally to a maximum temperature of 1000 °C at a fixed rate of 10 °C/min under a nitrogen (N₂) flow rate of 50 cm³/min. During the TGA operation, ongoing data on the sample weight and temperature were collected to determine the thermal stability and reaction mechanism by the curves of TGA and its derivative thermogravimetry (DTG). The TGA curve was normalized based on the weight of RH sample fed.

2.3. Pyrolysis Experiments

Based on the TGA/DTG data (discussed in Section 3.1), the pyrolysis temperature had to be above 400 °C because the peak temperature of DTG was found to be around 380 °C. This result was consistent with those reported by Johar et al. [34], indicating the complete devolatilization of hemicellulose and cellulose at around 400 °C. Therefore, the pyrolysis experiments were performed by the matrix combinations of temperature (400–900 °C, increased by the interval of 100 °C) and holding time (0–90 min, increased by the interval of 30 min) in the present study. Herein, a null holding time means that the heating was stopped (powered off) when the specified temperature was reached. Based on previous studies for producing biochar [35–40], a vertical fixed-bed electric furnace is suitable equipment for the production of biochar from various biomass feedstocks. For each pyrolysis experiment, around 5 g of the RH sample was pyrolyzed at a heating rate of around 10 °C/min under an inert atmosphere by passing N₂ flow rate of 500 cm³/min. The biochar yield was obtained from the difference between the initial RH sample weight and the resulting biochar weight based on the weight of RH sample fed. In order to describe the RH-based biochar (i.e., BRH), the resulting biochar was denoted as BRH-pyrolysis temperature-holding time. For example, the product BRH-400-30 refers to the pyrolysis conditions at temperature of 400 °C for holding time of 30 min.

2.4. Physicochemical Properties of Resulting Biochar

In this work, an accelerated surface area and porosimetry system (ASAP 2020; Micromeritics Co., USA) was used to determine the pore properties of the BRH products, including the Brunauer–Emmett–Teller (BET) surface area, pore volume and pore size distribution. Herein, the calculation of specific surface area was performed using the BET equation, using a range of relative pressure from 0.05 to 0.30. The total pore volume was taken as the nitrogen liquid volume adsorbed at a relative pressure of ca. 0.995. Using the *t*-plot method, the data on micropore area and micropore volume were obtained by the Halsey equation [41]. According to the definition by the International Union of Pure and Applied Chemistry (IUPAC) [41], micropores refer to pores with an internal diameter or width of less than 2 nm. Mesopores are defined as pores with an internal diameter or width between 2 and 50 nm. Regarding the pore size distributions of the BRH products,

the Barrett–Joyner–Halenda (BJH) method was employed to calculate them in the range of mesopores and small macropores from experimental N₂ isotherms (desorption branch) using the Kelvin model of pore filling [41].

The porosity of a material is defined as the ratio of the total pore volume to the apparent volume of the particle or powder (excluding inter-particle voids). Therefore, this property can be estimated by subtracting the ratio of particle (apparent or skeletal) density to true density from 1 [42,43]. In this work, a gas (helium) pycnometer (AccuPyc 1340; Micromeritics Co., USA) was used to determine the true density. Although mercury (Hg) porosimetry is often used to measure particle density due to the high surface tension of Hg, this property was estimated by using the measured data on the true density and total pore volume [43].

The textural morphology on the surface of the BRH product was observed by the SEM system (S-3000N; Hitachi Co., Japan). Prior to the SEM analysis, the BRH sample was coated by a conductive gold film using an ion sputter (E1010; Hitachi Co., Japan). An accelerating potential of 15.0 kV (electron beam) in a vacuum chamber was applied to the specimen surface during the SEM analysis. In addition, EDS analysis was used to quantify the elemental compositions rapidly and simply when scanning the BRH sample during the SEM analysis.

The oxygen-containing functional groups on the surfaces of the BRH products were analyzed by FTIR (FT/IR-4600; JASCO Co., Japan). Prior to the FTIR analysis, the dried BRH sample was mixed with spectroscopic-grade potassium bromide (KBr) powder, and then ground in an agate mortar. The finely uniform mixture (around 1 wt% BRH) was pressed in a hydraulic machine to form a disc with a diameter of ca. 1.2 cm and thickness of ca. 1 mm. The FTIR spectra were obtained by scanning with a wave number range of 4000–400 cm⁻¹ and a resolution of 4 cm⁻¹.

3. Results and Discussion

3.1. Thermogravimetric Analysis (TGA) of Rice Husk (RH)

As mentioned above, a pre-pyrolysis test of the RH sample was carried out by a thermal analyzer under an inert atmosphere at a fixed heating rate of 10 °C/min. The test conditions were very similar to the pyrolysis experiments for producing RH biochar. Figure 1 presents the TGA/TGA curves for the RH sample, showing that the significant degradation temperature was less than 400 °C. As shown, there were two apparent peaks and one shoulder as the pyrolysis temperature increased from room temperature to 400 °C. In the first peak, mass loss should occur in the form of water vapor (moisture) between 60 and 200 °C. For a lignocellulosic biomass, hemicellulose and a smaller amount of cellulose may be the most labile polymeric components as compared to lignin [1]. This implies that the TGA shoulder appeared at a temperature of around 300 °C, which is lower than that of lignin. During the stage of pyrolysis, the complex reactions (e.g., cracking, condensation) involve depolymerization and scission, thus causing a continual mass loss in the form of vapors such as moisture, CO₂ and volatile organics [44]. The final peak around 400 °C can be attributed to the thermal degradation of most cellulose and a smaller amount of lignin. In order to produce porous biochar from RH, the pyrolysis experiments thus started from 400 °C, where more lignin was pyrolyzed to form the products of char and tar. At higher temperatures (400–1000 °C), the mass loss can be attributed to the thermal degradation of most lignin and inorganic minerals (e.g., carbonates, chlorides, oxides) [26].

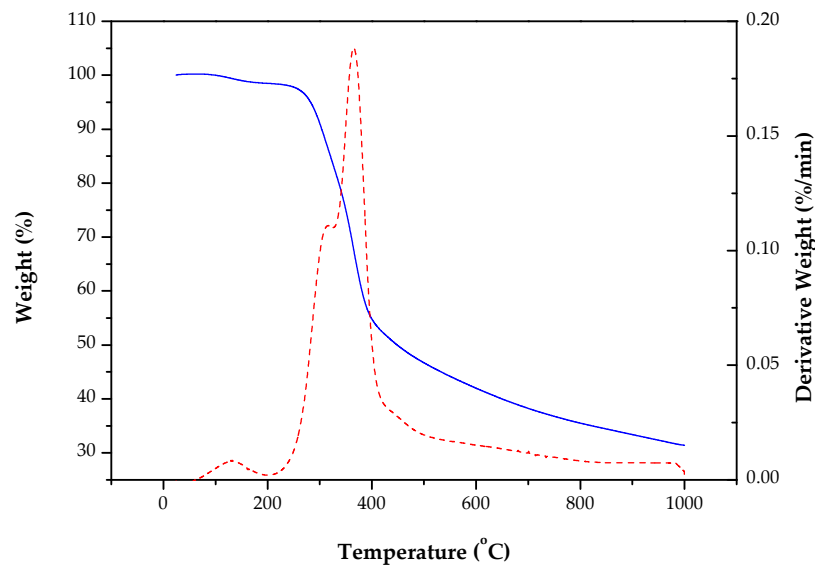


Figure 1. Thermogravimetric analysis (TGA) curve (blue color) and derivative thermogravimetry (DTG) curve (red dash line) of rice husk (RH) at a heating rate of 10 °C/min.

3.2. Yields and Pore Properties of Resulting Biochar

3.2.1. Yields of Resulting Biochar

The biochar yield was calculated by the ratio of biochar mass to RH mass loaded into each pyrolysis experiment (around 5 g). As the pyrolysis temperature increased, more condensable products were formed as water and organic components, but there remained less carbonized solids as biochar due to the complex degradation reactions in progress. Figure 2 illustrates the variation in the yield of the resulting RH-based biochar as a function of temperature (400–900 °C) for a holding time of 30 min, indicating a decreasing trend. Although not shown here, the yields of the resulting RH-based biochar prepared at 900 °C for four holding times (0, 30, 60 and 90 min) also indicated this trend.

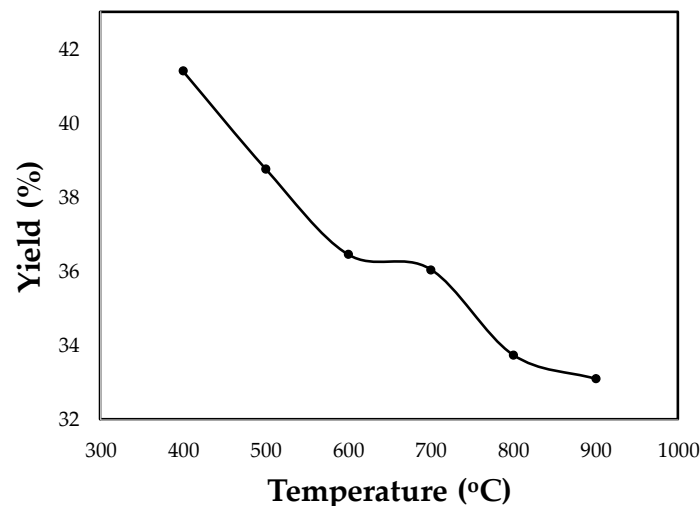


Figure 2. Variation in the yield of resulting RH-based biochar as a function of temperature.

3.2.2. Pore Properties of Resulting Biochar

The potential applications of biochar for water retention, sorption of contaminants and as a habitat for microorganisms are strongly dependent on its pore properties, which include specific surface area, density, porosity and morphology [45]. In the present study, all pore properties of the biochar samples were based on N₂ gas adsorption–desorption at −196 °C and helium gas displacement. Table 1 lists the pore properties of the resulting

biochar (BRH series), which included the BET surface area (S_{BET}), total pore volume (V_t), true density (ρ_s), particle density (ρ_p) and porosity (ε_p). Although particle density can be determined by a mercury (Hg) pycnometer due to the high surface tension of Hg and its inability to enter any pore of the porous sample [41], it was calculated by the values of total pore volume and true density in the present study [42].

$$\rho_p = \rho_s / (V_t \times \rho_s + 1) \quad (1)$$

Table 1. Pore properties of resulting RH-based biochar.

Biochar ^a	BET Surface Area ^b (m ² /g)	Total Pore Volume ^c (cm ³ /g)	True Density ^d (g/cm ³)	Particle Density ^e (g/cm ³)	Porosity ^f (–)
BRH-400-30	35.4	0.049	1.662	1.537	0.075
BRH-500-30	210.9	0.161	1.643	1.299	0.209
BRH-600-30	225.6	0.145	1.717	1.375	0.199
BRH-700-30	219.5	0.157	1.852	1.435	0.225
BRH-800-30	244.3	0.154	1.987	1.521	0.234
BRH-900-30	258.6	0.196	2.071	1.473	0.289
BRH-900-0	242.8	0.175	2.075	1.522	0.266
BRH-900-30	258.6	0.196	2.071	1.473	0.289
BRH-900-60	274.6	0.222	2.074	1.420	0.315
BRH-900-90	278.9	0.223	2.076	1.419	0.316

^a Sample notation indicated the resulting biochar (BRH-temperature-time) produced at the temperature of 400–900 °C for a holding time of 0–90 min using 5 g dried rice husk (RH). ^b BET surface area (S_{BET}) was based on relative pressure range of 0.05–0.30. ^c Total pore volume (V_t) was obtained at relative pressure of around 0.99. ^d True density (ρ_s) was measured by the helium displacement method. ^e Particle density (ρ_p) was calculated from the total pore volume (V_t) and true density (ρ_s). ^f Particle porosity (ε_p) was calculated from the particle density (ρ_p) and true density (ρ_s).

Furthermore, the porosity (ε_p) can be obtained by subtracting the ratio of particle density to true density from 1 [43]:

$$\varepsilon_p = 1 - (\rho_p / \rho_s) \quad (2)$$

As listed in Table 1, there were obvious variations in the pore properties of the biochar as a function of pyrolysis temperature (400–900 °C) and holding time (0–90 min). Similar to numerous studies [45,46], there was a positive correlation between the BET surface area (or porosity) and pyrolysis temperature. When the pyrolysis temperature increased from 400 to 900 °C, there was greater formation of pyrogenic amorphous biochar [27], thus causing a greater pore space or more pores with the pyrolysis temperature as charring intensity increased. Noticeably, the pore properties of the biochar continuously increased as the pyrolysis temperature increased up to 900 °C (for a fixed holding time of 30 min), or as the holding time was extended up to 90 min (at a fixed pyrolysis temperature of 900 °C). This implies that the structural breakdown of the resulting biochar produced at higher temperatures, probably due to sintering or fusion [45], was not observed in this work [47]. In the present study, the process parameter of pyrolysis temperature had a more significant effect on the pore properties of biochar as compared with the holding time (or reaction residence time). This is because the extent of physical changes (e.g., mass loss) for the biochar was highly dependent on the temperature during pyrolysis processing (seen in Figure 1). From the viewpoint of efficient energy use, the pyrolysis conditions at 500 °C for 30 min may be suitable for the production of RH-based biochar with a high BET surface area of 211 m²/g when compared with the resulting biochar (BET surface area of 279 m²/g) prepared at 900 °C for 90 min.

The BET surface area of the resulting biochar was also linked to its N₂ adsorption–desorption isotherms, which can be further transformed into its pore size distribution based on the BJH method [41]. Figure 3 depicts the N₂ adsorption–desorption isotherms and pore

size distributions of the resulting biochar prepared at various pyrolysis temperatures for a holding time of 30 min. Furthermore, Figure 4 shows the similar characteristics of the resulting biochars prepared at 900 °C for different holding times. As shown in Figures 3 and 4, the corresponding N₂ adsorption–desorption isotherms and pore size distributions of the resulting biochars were consistent with those in Table 1. Furthermore, the biochar pyrolyzed at higher temperatures showed more pronounced pore development, including micropores and mesopores. Therefore, these biochars possess the so-called Type I and Type-IV shapes (isotherms) [41]. This mesoporous feature will be beneficial in providing water retention, adsorption capacity and microbial growth space.

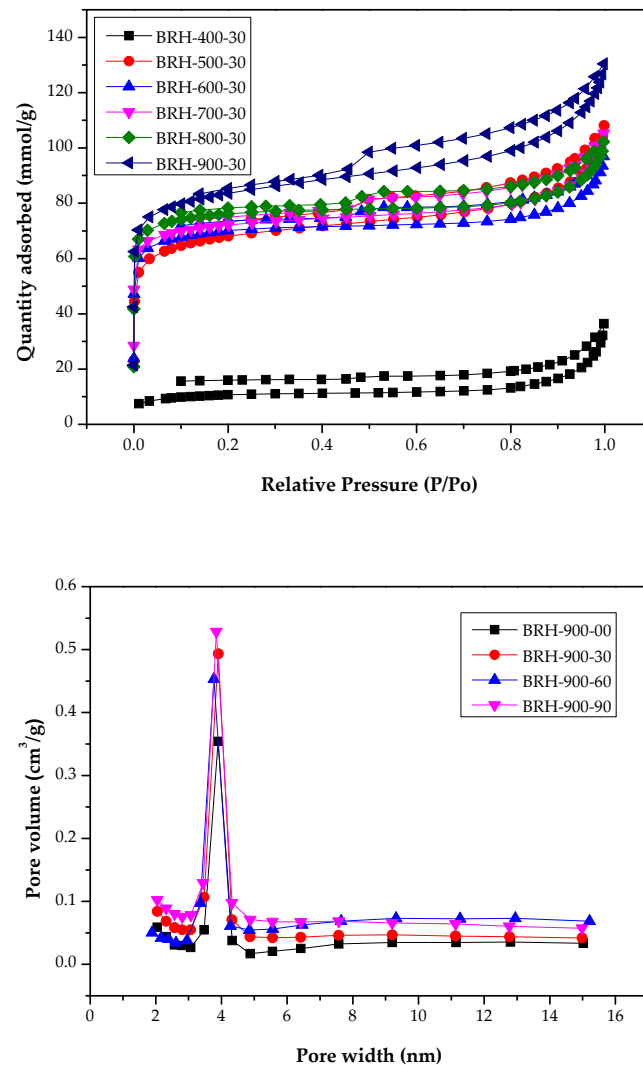


Figure 3. N₂ adsorption–desorption isotherms (**upper**) and pore size distributions (**lower**) of resulting biochar prepared at various temperatures for a fixed holding time of 30 min.

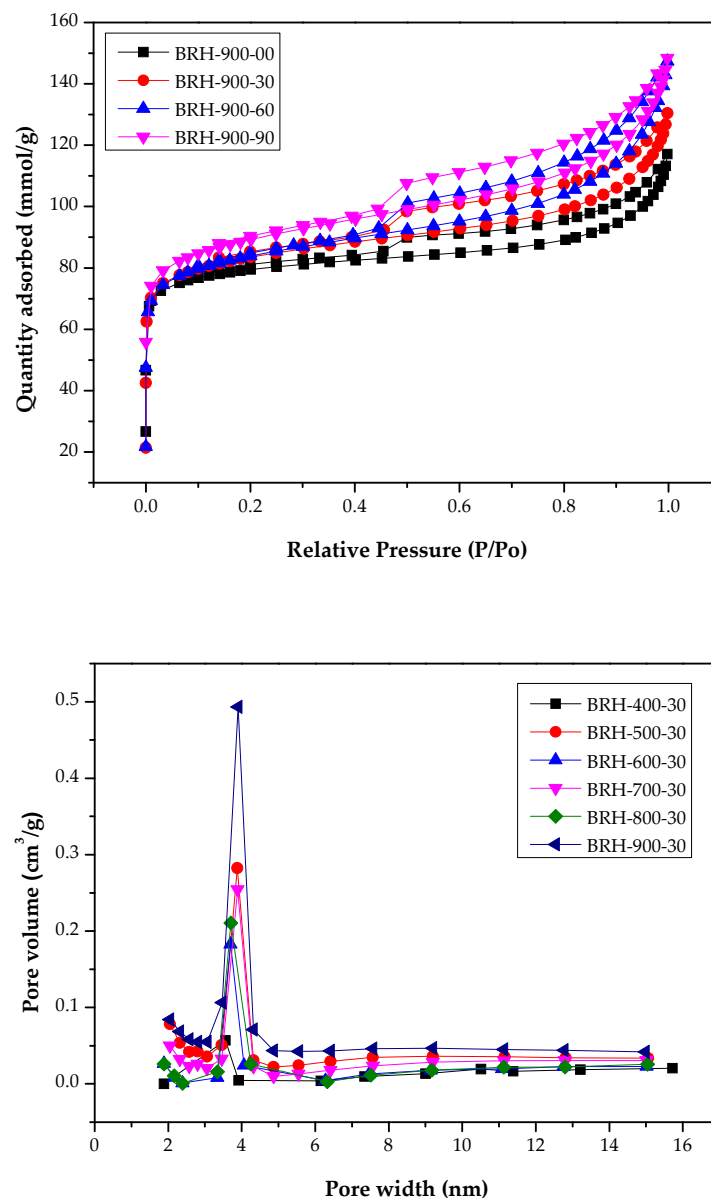


Figure 4. N_2 adsorption–desorption isotherms (**upper**) and pore size distributions (**lower**) of resulting biochar prepared at 900 °C for various holding times.

In order to observe the porous texture of the resulting biochar, SEM analyses at 15 kV were performed on its gold-coated surface with different magnifications (i.e., 200 and 1000). As shown in the SEM images (Figure 5), the representative biochar (i.e., BRH-900-30) has fine pores on the surface. These pores will be more formed from gas vesicles at higher pyrolysis temperatures, resulting in better pore properties such as specific surface area and porosity (Table 1). In addition, the resulting biochar also exhibits a rigid, irregular and rough surface due to its rigid silica composition and the rigorous carbonization at a higher temperature (i.e., 900 °C) for a longer holding time (i.e., 30 min). In this regard, the RH-based biochar may be a good medium for possible applications in water retention and wastewater treatment in the soil environment due to its highly porous structure.

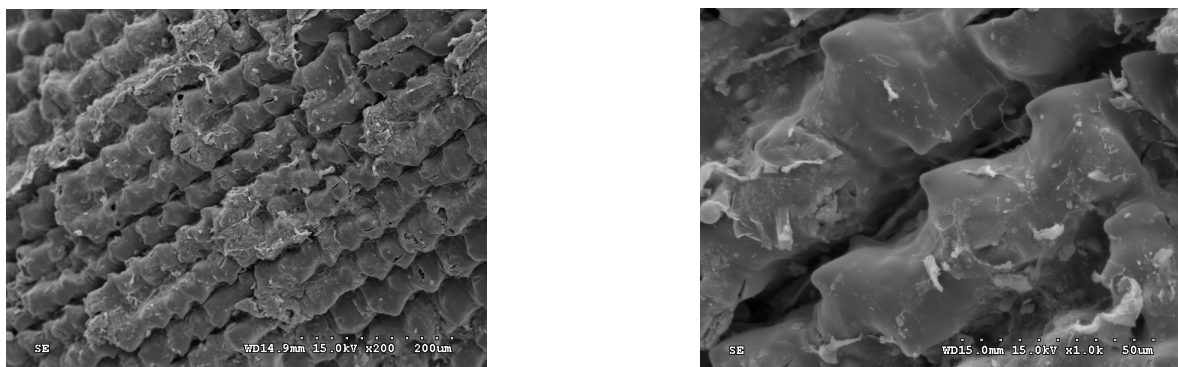


Figure 5. SEM images ($\times 200$, left; $\times 1000$, right) of the resulting biochar (BRH-900-30).

3.3. Chemical Characterization of Resulting Biochar

As described in Section 2.4, the EDS system, which is commonly used alongside SEM, was used to enable semi-quantitative elemental analysis on the surface of the resulting biochar. Figure 6 shows an EDS spectrum from the resulting biochar (BRH-900-30), observing the presence of carbon (C), oxygen (O) and silicon (Si). As a preliminary quantification, the corresponding contributions to the elemental composition are 18.15, 4.66 and 40.19 wt%, respectively. The presence of C and O in the RH-based biochar should arise from its lignocellulosic precursor (i.e., RH). The most significant peak is assigned to the presence of Si due to the high content of silica (SiO_2) in the RH. The rich presence of silica in the RH-based biochar can be further identified by X-ray diffraction (XRD) [48] or X-ray photoelectron spectroscopy (XPS) analysis [49].

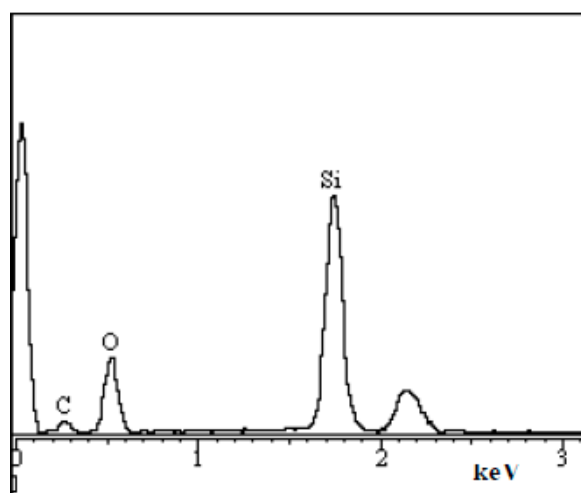


Figure 6. EDS spectrum of the resulting biochar (BRH-900-30).

In general, the chemical characteristics of biochar mainly comprise aromatic C and inorganic minerals, which are dependent on the starting feedstock and pyrolysis conditions applied. The presence of functional groups on the surface of biochar plays a vital role in the soil and water environments. For example, the addition of biochar to soil has been proven to enhance the sorption capacities for heavy metal ions by the electrostatic attraction [45], which can be attributed to the high contents of oxygen-containing functional groups on the surface due to the negatively charged surface. The FTIR spectrum of the resulting biochar (BRH-900-30) shown in Figure 7 has the following features [23,50,51]. The peak at 3460 cm^{-1} can be assigned to the presence of adsorbed water and hydrogen-bonded biochar O-H groups. The band between 1500 and 1700 cm^{-1} could be attributed to C=O stretching or C=C groups in aromatic rings. The sharp peak around 1385 cm^{-1} could be assigned to the symmetric deformation band of $-\text{CH}_3$ groups. The peak at around

1115 cm^{-1} could be the stretching vibration of C-O and the vibration of silica bonds. Si-O framework bands at around 1115 cm^{-1} and below 800 cm^{-1} were evident [17]. These FTIR results were in accordance with those in the EDS analysis (Figure 6), enhancing the slight hydrophilicity on the surface of the RH-based biochar. These functional groups will impact the soil pH and interaction with ionic contaminants in soil, causing higher cation exchange capacity (CEC) and adsorption capacities for cations (e.g., metal ions).

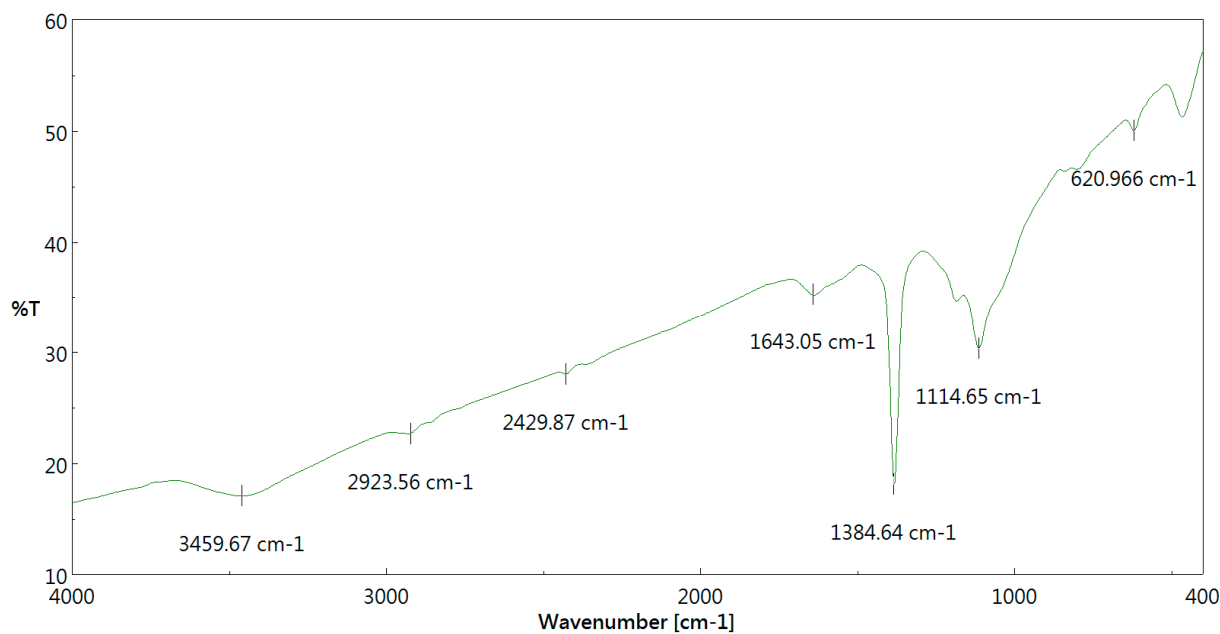


Figure 7. FTIR spectrum of the resulting biochar (BRH-900-30).

4. Conclusions

In this work, a series of biochars were prepared from RH at various pyrolysis conditions, which were designed by the matrix of temperature (400–900 °C) and holding times (i.e., 0–90 min) based on the results of a pre-pyrolysis test by TGA. The pore properties (i.e., BET surface area and porosity) of the resulting RH-based biochar were clearly positively linked to the studied ranges of pyrolysis temperature and holding time. The maximal pore properties with the BET surface area of around 280 m^2/g could be obtained from the conditions at 900 °C for a holding time of 90 min. The porosity of the optimal biochar was as high as 0.316. In addition, the resulting biochar showed characteristic of microporous and mesoporous structures based on the N_2 adsorption–desorption isotherms and pore size distributions. The results of the EDS and FTIR analyses also supported the slight hydrophilicity on the surface of the RH-based biochar due to the richness in oxygen/silica-containing functional groups. Based on the physicochemical properties determined, the RH-based biochar could be an excellent material for possible applications in water conservation, wastewater treatment and soil amendment.

Author Contributions: Conceptualization, W.-T.T.; methodology, Y.-Q.L. and H.-J.H.; validation, Y.-Q.L. and H.-J.H.; data curation, Y.-Q.L.; formal analysis, Y.-Q.L.; resources, Y.-Q.L.; writing—original draft preparation, W.-T.T.; writing—review and editing, W.-T.T.; supervision, W.-T.T. All authors have read and agreed to the published version of the manuscript.

Funding: This research received no external funding.

Institutional Review Board Statement: Not applicable.

Informed Consent Statement: Not applicable.

Data Availability Statement: Not applicable.

Acknowledgments: The authors express sincere thanks to the Instrument Center of National Pingtung University of Science and Technology for the assistance in the scanning electron microscope (SEM)/energy-dispersive X-ray spectroscopy (EDS) analysis. Additionally, the authors are thank Ming-Shou Tang, Chin-Hsien Chang and Tsung-Hsien Kuo (undergraduate students at the Department of Environmental Engineering and Science) for conducting the pyrolysis experiments.

Conflicts of Interest: The authors declare no conflict of interest.

References

1. Basu, P. *Biomass Gasification, Pyrolysis and Torrefaction*, 2nd ed.; Academic Press: San Diego, CA, USA, 2013.
2. Demirbas, A. Biomass resource facilities and biomass conversion processing for fuels and chemicals. *Energy Convers. Manag.* **2001**, *42*, 1357–1378. [[CrossRef](#)]
3. Lehmann, J.; Joseph, S. Biochar for environmental management: An introduction. In *Biochar for Environmental Management*, 2nd ed.; Lehmann, J., Joseph, S., Eds.; Routledge: New York, NY, USA, 2015; pp. 1–13.
4. Dai, Y.J.; Zhang, N.X.; Xing, C.M.; Cui, Q.X.; Sun, Q.Y. The adsorption, regeneration and engineering applications of biochar for removal organic pollutants: A review. *Chemosphere* **2019**, *223*, 12–27. [[CrossRef](#)] [[PubMed](#)]
5. Zhang, Z.K.; Zhu, Z.Y.; Shen, B.X.; Liu, L.N. Insights into biochar and hydrochar production and applications: A review. *Energy* **2019**, *171*, 581–598. [[CrossRef](#)]
6. Wang, J.; Wang, S. Preparation, modification and environmental application of biochar: A review. *J. Clean. Prod.* **2019**, *227*, 1002–1022. [[CrossRef](#)]
7. Fdez-Sanroman, A.; Pazos, M.; Rosales, E.; Sanroman, M.A. Unravelling the environmental application of biochar as low-cost biosorbent: A review. *Appl. Sci.* **2020**, *10*, 7810. [[CrossRef](#)]
8. Shan, R.; Han, J.; Gu, J.; Yuan, H.R.; Luo, B.; Chen, Y. A review of recent developments in catalytic applications of biochar-based materials. *Resour. Conserv. Recycl.* **2020**, *162*, 105036. [[CrossRef](#)]
9. Wang, D.; Jiang, P.K.; Zhang, H.B.; Yuan, W. Biochar production and applications in agro and forestry systems: A review. *Sci. Total Environ.* **2020**, *723*, 137775. [[CrossRef](#)]
10. Food and Agriculture Organization FAOSTAT. Available online: <http://www.fao.org/faostat/en/#data/QC/visualize> (accessed on 18 March 2021).
11. Council of Agriculture (COA). *Agriculture Statistics Yearbook*; COA: Taipei, Taiwan, 2020.
12. Jenkins, B.M.; Baxter, L.L.; Miles, T.R., Jr.; Miles, T.R. Combustion properties of biomass. *Fuel Process. Technol.* **1998**, *54*, 17–46. [[CrossRef](#)]
13. Moraes, C.A.M.; Fernandes, I.J.; Calheiro, D.; Kieling, A.G.; Brehm, F.A.; Rigon, M.R.; Fiho, J.A.B.; Schneider, I.A.H.; Osorio, E. Review of the rice production cycle: By-products and the main applications focusing on rice husk combustion and ash recycling. *Waste Manag. Res.* **2014**, *32*, 1034–1048. [[CrossRef](#)]
14. Soltani, N.; Bahrami, A.; Pech-Canul, M.I.; Gonzalez, L.A. Review on the physicochemical treatments of rice husk for production of advanced materials. *Chem. Eng. J.* **2015**, *264*, 899–935. [[CrossRef](#)]
15. Quispe, I.; Navia, R.; Kahhat, R. Energy potential from rice husk through direct combustion and fast pyrolysis: A review. *Waste Manag.* **2017**, *59*, 200–210. [[CrossRef](#)] [[PubMed](#)]
16. Vassileva, P.; Detcheva, A.; Uzunov, I.; Uzunova, S. Removal of metal ions from aqueous solutions using pyrolyzed rice husks: Adsorption kinetics and equilibria. *Chem. Eng. Comm.* **2013**, *200*, 1578–1599. [[CrossRef](#)]
17. Jindo, K.; Mizumoto, H.; Sanchez-Monedero, M.A.; Sonoki, T. Physical and chemical characterization of biochars derived from different agricultural residues. *Biogeosciences* **2014**, *11*, 6613–6621. [[CrossRef](#)]
18. Phuong, H.T.; Uddin, M.A.; Kato, Y. Characterization of biochar from pyrolysis of rice husk and rice straw. *J. Biobased Mater. Bioenergy* **2015**, *9*, 439–446. [[CrossRef](#)]
19. Ahiduzzaman, M.; Sadrul Islam, A. Preparation of porous bio-char and activated carbon from rice husk by leaching ash and chemical activation. *SpringerPlus* **2016**, *5*, 1248. [[CrossRef](#)] [[PubMed](#)]
20. Wei, L.; Huang, Y.; Li, Y.; Huang, L.; Mar, N.N.; Huang, Q.; Liu, Z. Biochar characteristics produced from rice husks and their sorption properties for the acetanilide herbicide metolachlor. *Environ. Sci. Pollut. Res.* **2017**, *24*, 4552–4561. [[CrossRef](#)] [[PubMed](#)]
21. Zhang, Y.; Ma, Z.; Zhang, Q.; Wang, J.; Ma, Q.; Yang, Y.; Luo, X.; Zhang, W. Comparison of the physicochemical characteristics of bio-char pyrolyzed from moso bamboo and rice husk with different pyrolysis temperatures. *BioResources* **2017**, *12*, 4652–4669. [[CrossRef](#)]
22. Dissanayake, D.K.R.P.L.; Dharmakeerthi, R.S.; Karunaratna, A.K.; Dandeniya, W.S. Changes in structural and chemical properties of rice husk biochar co-pyrolysed with Eppawala rock phosphate under different temperatures. *Trop. Agric. Res.* **2018**, *30*, 19–31. [[CrossRef](#)]
23. Jia, Y.; Shi, S.; Liu, J.; Su, S.; Liang, Q.; Zeng, X.; Li, T. Study of the effect of pyrolysis temperature on the Cd²⁺ adsorption characteristics of biochar. *Appl. Sci.* **2018**, *8*, 1019. [[CrossRef](#)]
24. Shi, J.; Fan, X.; Tsang, D.C.W.; Wang, F.; Shen, Z.; Hou, D.; Alessi, D.S. Removal of lead by rice husk biochars produced at different temperatures and implications for their environmental utilizations. *Chemosphere* **2019**, *235*, 825–831. [[CrossRef](#)]
25. Singh, S.V.; Chaturvedi, S.; Dhyan, V.C.; Kasivelu, G. Pyrolysis temperature influences the characteristics of rice straw and husk biochar and sorption/desorption behaviour of their biourea composite. *Bioresour. Technol.* **2020**, *314*, 123674. [[CrossRef](#)] [[PubMed](#)]

26. Saeed, A.A.H.; Harun, N.Y.; Sufian, S.; Afolabi, H.K.; Al-Qadami, E.H.H.; Roslan, F.A.S.; Rahim, S.A.; Ghaleb, A.A.S. Production and characterization of rice husk biochar and Kenaf biochar for value-added biochar replacement for potential materials adsorption. *Ecol. Eng. Environ. Technol.* **2021**, *22*, 1–8. [[CrossRef](#)]
27. Keiluweit, M.; Nico, P.S.; Johnson, M.G.; Kleber, M. Dynamic molecular structure of plant biomass-derived black carbon (biochar). *Environ. Sci. Technol.* **2010**, *44*, 1247–1253. [[CrossRef](#)]
28. Rossi, M.M.; Silvani, L.; Amanat, N.; Papini, M.P. Biochar from pine wood, rice husks and iron-*Eupatorium* shrubs for remediation applications: Surface characterization and experimental tests for trichloroethylene removal. *Materials* **2021**, *14*, 1776. [[CrossRef](#)]
29. Harun, N.S.N.; Jaafar, N.M.; Sakimin, S.Z. The effects of rice husk biochar rate on arbuscular mycorrhizal fungi and growth of soursop (*Annona muricata* L.) seedlings. *Sustainability* **2021**, *13*, 1817. [[CrossRef](#)]
30. Tsai, C.C.; Chang, Y.F. Effects of rice husk biochar on carbon release and nutrient availability in three cultivation age of greenhouse soils. *Agronomy* **2020**, *10*, 990. [[CrossRef](#)]
31. Selvarajh, G.; Ch'ng, H.Y.; Md Zain, N.; Sannasi, P.; Mohammad Azmin, S.N.H. Improving soil nitrogen availability and rice growth performance on a tropical acid soil via mixture of rice husk and rice straw biochars. *Appl. Sci.* **2021**, *11*, 108. [[CrossRef](#)]
32. Tsai, C.C.; Chang, Y.F. Carbon dynamics and fertility in biochar-amended soils with excessive compost application. *Agronomy* **2019**, *9*, 511. [[CrossRef](#)]
33. Tsai, W.T.; Lee, M.K.; Chang, Y.M. Fast pyrolysis of rice husk: Product yields and compositions. *Bioresour. Technol.* **2007**, *98*, 22–28. [[CrossRef](#)]
34. Johar, N.; Ahmad, I.; Dufresne, A. Extraction, preparation and characterization of cellulose fibres and nanocrystals from rice husk. *Ind. Crops Prod.* **2012**, *37*, 93–99. [[CrossRef](#)]
35. Touray, N.; Tsai, W.T.; Chen, H.L.; Liu, S.C. Thermochemical and pore properties of goat-manure-derived biochars prepared from different pyrolysis temperatures. *J. Anal. Appl. Pyrolysis* **2014**, *109*, 116–122. [[CrossRef](#)]
36. Tsai, W.T.; Huang, C.N.; Chen, H.R.; Cheng, H.Y. Pyrolytic conversion of horse manure into biochar and its thermochemical and physical properties. *Waste Biomass Valori.* **2015**, *6*, 975–981. [[CrossRef](#)]
37. Liu, S.C.; Tsai, W.T. Thermochemical characteristics of dairy manure and its derived biochars from a fixed-bed pyrolysis. *Int. J. Green Energy* **2016**, *13*, 963–968. [[CrossRef](#)]
38. Hung, C.Y.; Tsai, W.T.; Chen, J.W.; Lin, Y.Q.; Chang, Y.M. Characterization of biochar prepared from biogas digestate. *Waste Manag.* **2017**, *66*, 53–60. [[CrossRef](#)]
39. Tsai, C.H.; Tsai, W.T.; Liu, S.C.; Lin, Y.Q. Thermochemical characterization of biochar from cocoa pod husk prepared at low pyrolysis temperature. *Biomass Convers. Biorefin.* **2018**, *8*, 237–243. [[CrossRef](#)]
40. Tsai, W.T.; Huang, C.P.; Lin, Y.Q. Characterization of biochars produced from dairy manure at high pyrolysis temperatures. *Agronomy* **2019**, *9*, 634. [[CrossRef](#)]
41. Lowell, S.; Shields, J.E.; Thomas, M.A.; Thommes, M. *Characterization of Porous Solids and Powders: Surface Area, Pore Size and Density*; Springer: Dordrecht, The Netherlands, 2006.
42. Smith, J.M. *Chemical Engineering Kinetics*, 3rd ed.; McGraw-Hill: New York, NY, USA, 1981.
43. Suzuki, M. *Adsorption Engineering*; Elsevier: Amsterdam, The Netherlands, 1990.
44. Masek, O.; Johnston, C.T. Thermal analysis for biochar characterisation. In *Biochar: A Guide to Analytical Methods*; Singh, B., Camps-Arbestain, M., Lehmann, J., Eds.; CRC Press: Boca Raton, FL, USA, 2017; pp. 283–293.
45. Mukome, F.N.D.; Parikh, S.J. Chemical, physical, and surface characterization of biochar. In *Biochar: Production, Characterization, and Applications*; Ok, Y.S., Uchimiya, S.M., Chang, S.X., Bolan, N., Eds.; CRC Press: Boca Raton, FL, USA, 2016; pp. 67–96.
46. Chia, C.H.; Downie, A.; Munroe, P. Characteristics of biochar: Physical and structural properties. In *Biochar for Environmental Management*, 2nd ed.; Lehmann, J., Joseph, S., Eds.; Routledge: New York, NY, USA, 2015; pp. 89–137.
47. Brown, R.A.; Kerche, A.K.; Nguyen, T.H.; Nagle, D.C.; Ball, W.P. Production and characterization of synthetic wood chars for use as surrogates for natural sorbents. *Org. Geochem.* **2006**, *37*, 321–333. [[CrossRef](#)]
48. Singh, B.; Raven, M.D. X-ray diffraction analysis of biochar. In *Biochar: A Guide to Analytical Methods*; Singh, B., Camps-Arbestain, M., Lehmann, J., Eds.; CRC Press: Boca Raton, FL, USA, 2017; pp. 245–252.
49. Smith, G.C. X-ray photoelectron spectroscopy analysis of biochar. In *Biochar: A Guide to Analytical Methods*; Singh, B., Camps-Arbestain, M., Lehmann, J., Eds.; CRC Press: Boca Raton, FL, USA, 2017; pp. 229–244.
50. Johnston, C.T. Biochar analysis by Fourier-transform infra-red spectroscopy. In *Biochar: A Guide to Analytical Methods*; Singh, B., Camps-Arbestain, M., Lehmann, J., Eds.; CRC Press: Boca Raton, FL, USA, 2017; pp. 199–228.
51. Islam, M.S.; Ang, B.C.; Gharekhani, S.; Afifi, A.B.M. Adsorption capability of activated carbon synthesized from coconut shell. *Carbon Lett.* **2016**, *20*, 1–9. [[CrossRef](#)]